

Snowflake: A Distributed Streaming Decoder

Tim Chan

Department of Materials, University of Oxford, Parks Road, Oxford OX1 3PH, United Kingdom

We design *Snowflake*, a quantum error correction decoder that, for the surface code under circuit-level noise, is roughly 25% more accurate than the Union–Find decoder, with a better mean runtime scaling: subquadratic as opposed to cubic in the code distance. Our decoder runs in a streaming fashion and has a local implementation. In designing *Snowflake*, we propose a new method for general stream decoding that eliminates the processing overhead due to window overlap in existing windowing methods.

1 Introduction

Decoders are crucial to the quantum error correction that enables fault-tolerant quantum computing. These classical algorithms must decode, i.e. infer errors from measurements and fix them, accurately and extremely quickly to clean the quantum computer faster than it corrupts. It is difficult to design a decoder sufficiently accurate, fast, and practical to implement in hardware [1–3]. This last requirement has led to interest in decoders that are local i.e. running on a grid of identical processors, each communicating only with their nearest neighbours [4–12]. Such decoders benefit from parallelism [13, §III.D], repairability [14, §3], reduced signal losses [15, pp 6–7], and lower latency [1, §VI] [16, §4.2] when used with local (requiring no long-range qubit–qubit interactions) codes.

A relatively new candidate gaining in popularity [2, 17–27] is the Union–Find decoder (UF) [28, 29]. Recent literature has explored UF implementations of varying levels of locality [14, 30–33], the first being *Helios* [34]. The closely related *Macar* [14] exhibits very similar runtime behaviour to *Helios*, and is the implementation we will repeatedly refer to for comparison. These implementations, save *Helios*, tackled only the batch decoding problem: a simplification of the stream decoding problem that actually occurs in practice. Relatively little work has gone into the latter: since 2002, two methods have been proposed allowing most batch decoders to be used as stream decoders. These are the commonly used *forward method* [35, §VI.B] and the newer *sandwich method* [36, 37], using the terminology of [37].

Tim Chan: timothy.chan@materials.ox.ac.uk

We design *Snowflake*, a generalisation of the local decoders in [14] from the batch to the streaming case. *Snowflake* comprises a simple set of local rules with very little central management, and works for any error-correcting code with a decoding graph embeddable in \mathbb{R}^3 without ‘long-range’ edges. Examples include the repetition code and the surface code under circuit-level noise. *Snowflake* relies on the new *frugal method* we develop for general stream decoding. This is similar to the forward method, but differs in that it discards none of the computation – it is more frugal with resources. This halves both the power draw and the size of the decoder architecture. We hope the proposal of this method enables the development of more streaming decoders.

When tested on the surface code under circuit-level noise, *Snowflake* recovers $\approx 97\%$ of the threshold of UF adapted with the forward method [which we abbreviate as FM(UF)], but in absolute terms is 24.9(5)% more accurate. Moreover, *Snowflake*’s mean runtime scaling with the code distance d improves upon original UF. *Snowflake* has a distributed implementation that is modular and scalable. This is a 3D lattice of processors though we note an alternative architecture that ‘flattens’ this lattice onto a 2D grid would be even more practical given current chip design capabilities, at a potentially marginal cost in speed.

Section 2 covers the prerequisite theory. We describe the frugal method in **Section 3**, explain *Snowflake* in **Section 4**, then numerically test its accuracy and runtime in **Section 5**. We conclude in **Section 6** and discuss how *Snowflake* may be implemented on a 2D chip and decode not just quantum memory but lattice surgery-based computation. In all figures, save **Figs. 6 to 11**, the time axis points upward. Our emulation code is on GitHub at [38].

2 Background

Section 2.1 recaps the batch decoding problem that has been previously explained in e.g. [14, §2.1]. In **Section 2.2** we generalise to the streaming case and in **Section 2.3** we provide one solution approach that already exists in literature.

2.1 The Batch Decoding Problem

The *decoding graph* G is defined by the code and the noise model (we explain how in **Appendix A**).

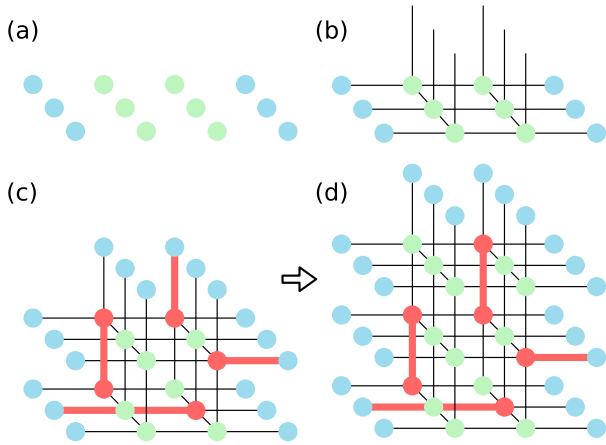


Figure 1: Defects are red nodes; other detectors, green; boundary nodes, blue. Bitflipped edges are thick and red; else, thin and black. (a) A sheet and (b) a layer of (c) the decoding graph for the surface code under phenomenological noise. (d) How said graph changes after one measurement round: one layer is added on top. This is the streaming analogue of the batch version in [14, Figure 3b]; note the addition of a temporal boundary.

Its nodes fall into two types: *detectors* and *boundary nodes*. Each edge is, at any given time, either bitflipped or not bitflipped; this property is not known to the decoder, though it *can* apply bitflips (and of course keep track of which edges it has applied bitflips to).

In a *decoding cycle*, each edge becomes bitflipped with some potentially unique probability that is a function of a universal noise level p .

Definition 1. A *defect* is a detector touching an odd number of bitflipped edges.

The *syndrome* \mathbb{S} is the set of defects. Knowing only \mathbb{S} , the decoder must bitflip more edges, thus modifying \mathbb{S} , until $\mathbb{S} = \emptyset$. The decoding cycle ends here. Formally, be the *correction* \mathbb{C} the final set of edges the decoder chooses to bitflip; then \mathbb{C} must *annihilate all defects* i.e. constitute paths that pair each defect with either another defect or a boundary node.

The boundary nodes are partitioned into two *spatial boundaries*. A path of bitflipped edges connecting them is called a *logical bitflip*; the shortest such path has d edges. We evaluate decoder accuracy by the probability a single batch fails i.e. a single decoding cycle ends with an odd number of logical bitflips left over.

2.2 The Stream Decoding Problem

Whereas the batch decoding problem was defined for three noise models, this problem is defined for only two of them: phenomenological and circuit-level.

Figure 1ab illustrates the following definitions: a *sheet* is a subset of nodes of G with the same t co-

ordinate; a *layer*, the periodic unit subgraph of G . For the stream decoding problem, there are an *indefinite* number of measurement rounds; this means new layers are constantly being added to the top of G as in Fig. 1cd. In general, some edges in the new layer are bitflipped (specifically, the bitflip probability for each edge equals that of the analogous edge in the layer below), creating defects in the new layer. The decoder must constantly add to \mathbb{C} to annihilate these new defects.

We evaluate decoder accuracy by the below metric which is a reasonable streaming analogue to the batch failure probability [39, §VI].

Definition 2. The *logical error rate* is the logical bitflip count per d measurement rounds.

For clarity, all figures in the rest of this paper, save Figs. 6 to 11, use a planar G corresponding to the repetition code under phenomenological noise. However, the same concepts apply to other graphs such as for the surface code under circuit-level noise.

2.3 Forward Method

This method was first proposed in [35, §VI.B] as the ‘overlapping recovery method’ but a more detailed explanation can be found in [36, pp 2–3] where it is called ‘sliding window decoding’. It has been applied to the general class of *quantum low-density parity-check codes* (LDPC, which includes the repetition and surface codes) [40–43]. It reduces the stream decoding problem to batch decoding by chunking the syndrome, decoding each chunk, then stitching together all the corrections. The chunks must overlap, else a small defect pair could straddle two consecutive chunks hence be decoded inaccurately.

More concretely, assume G already comprises many layers. This method, illustrated in Fig. 2, relies on a ‘viewing window’ W that is at any given time a subgraph comprising $c+b$ consecutive layers of G . The lowest c layers of W is always defined as the *commit region*; the rest, the *buffer region*. W starts at the bottom, i.e. as the lowest $c + b$ layers, of G . The method then indefinitely repeats the *decoding cycle*, here defined as the following:

1. Use any batch decoder to find a *tentative correction* \mathbb{T} that annihilates all defects seen in W .
2. Add to \mathbb{C} the part of \mathbb{T} in the commit region, and forget the rest.
3. Raise W by c layers i.e. redefine it as the subgraph that is c layers higher.

Since b ‘layers of computation’ are forgotten per decoding cycle, decoding τ sheets of syndrome data discards a total of $\approx b\tau/c$ layers of computation. If the bitflip probabilities of all edges of G are of the same order, we need the chunk overlap $b \gtrsim d$ to ensure no

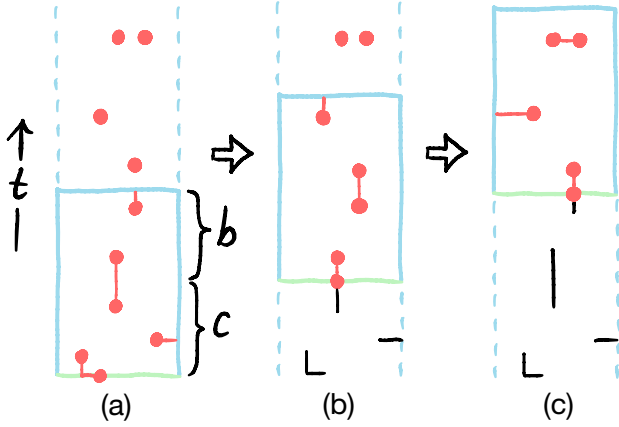


Figure 2: Two decoding cycles of the forward method. The viewing window is the solidly outlined rectangle with boundaries in blue. Defects are red dots. Tentative corrections are red lines; edges bitflipped by the decoder, black lines. The commit and buffer region heights are c and b , respectively. (a) The tentative correction contains a path that spans both regions. (b) This path is partially committed which makes an ‘artificial defect’ at the bottom of the new window that must also be annihilated. (c) The rest of the path is committed.

loss in accuracy [44, §IV.D]. Moreover, c cannot be too large else W becomes too tall leading to slow decoding cycles or in the case of a lookup-table decoder, high memory requirements. The most common choice thus is $c = b = d$ though others have been explored e.g. $0 \leq b < d$ [3, §3] [37, §B.2] [44, §VII.C] [45, §V.B] or $c = 1$ [46, §5.1] [41, 42]. In almost all cases, a considerable amount of computation is discarded. This is true for the sandwich method too as it also requires overlapping windows.

Remark 1. Having a temporal boundary at the top of W improves decoding accuracy [37, §B.3] as it allows the decoder to account for small defect pairs that straddle this boundary like the one in Fig. 2a. By tentatively pairing the known defect to the temporal boundary, the decoder delays the decision on how to properly annihilate it until it discovers the other defect just above in Fig. 2b. The same occurs with another defect near the top of this W , but this time it turns out there are no nearby defects above, so it is instead paired to a spatial boundary in Fig. 2c.

3 Frugal Method

Our alternative to the forward method differs from it in three ways:

1. \mathbb{T} need only satisfy the following.

Condition 1. \mathbb{T} is *complete*, i.e. annihilates all defects, within the commit region.

This is as opposed to being complete in *all* of W .

2. The decoder bitflips *all* edges in \mathbb{T} , modifying \mathbb{S} even in the buffer region during **step 1**. This

has no physical consequence for qubits as \mathbb{C} is ultimately only tracked by classical electronics in the so-called *Pauli frame* [47, 48].

3. The computation associated with the buffer region is not forgotten but used as a starting point for, and further developed in, the next decoding cycle.

As computation is never discarded, the power draw and thus heat generated by the device is minimised. This is vital for an on-chip, local decoder integrated with the qubits, as most qubit platforms demand low temperatures. Compared to the forward method for $c = b$, where 1 layer of computation is discarded per sheet of syndrome data, the power draw is halved.

In *hard* real-time decoding, the decoder is given a hard time limit for each decoding cycle, which should be set to no longer than c ancilla qubit measurement intervals. If it exceeds this limit, it is interrupted and the logical qubit is assumed to fail. On the other hand, *soft* real-time decoding demands less by introducing a buffer (in the conventional sense) between the newest measurement data and the top of W , in which case only *an average* decoding cycle would need to complete faster than c intervals; any slower then the backlog of syndrome data grows indefinitely [13, p 326]. In practice, decoding will likely be a hard real-time system [16, §2.1]. We analyse both individual and mean runtime for Snowflake in Section 5.2.

For the rest of the paper we set $c = 1$, which we can do for free as computation is never discarded. In this case the method becomes local (provided the decoder itself is local) as, from the perspective of W , data shifts down by *one layer* when W is raised. The commit region is also one layer thick, so the part of \mathbb{C} here can be offloaded from the bottom of W locally. Conceptually, this makes the method much more granular in nature.

4 Snowflake

Figure 3 illustrates how our local decoder finds \mathbb{T} . The algorithm is inspired by UF and explained by analogy to snowfall. As snowflakes fall they gradually grow. If two snowflakes touch they merge i.e. become one. In the same way, an active cluster nucleates at each new defect at the top of W and grows as it fall through W . If two clusters touch they merge.

A cluster stops growing if it inactivates. We use the following lemma from [14, §A.2].

Lemma 1. *A cluster is inactive iff it has an even defect count or touches a boundary.*

To determine the first condition, we push all defects to a unique point in the cluster called the *root*: a boundary if available; else, a highest point. When two defects meet they annihilate, so eventually zero

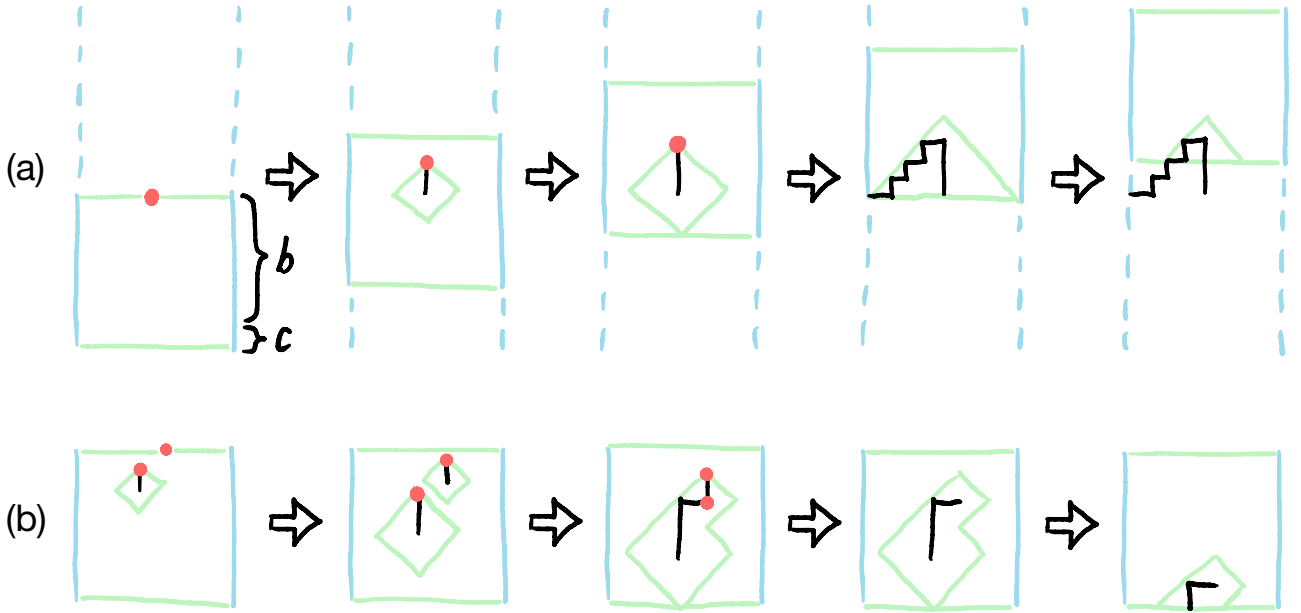


Figure 3: Two examples of Snowflake in action. Features are shown as in Fig. 2 and additionally, clusters are outlined in green. (a) A cluster grows around one defect as the window is raised, while the defect is always pushed to the highest point. As soon as the cluster touches a boundary, the defect is instead pushed to that boundary. This inactivates the cluster so it stops growing. It gradually disappears from view. (b) Two defects separated in time and space (this time viewed from the perspective of the window so clusters appear to fall). The lower cluster is older, hence larger, when both clusters merge. Frame 3 shows the lower defect on its way to the highest point to annihilate with the other defect, inactivating the resultant cluster.

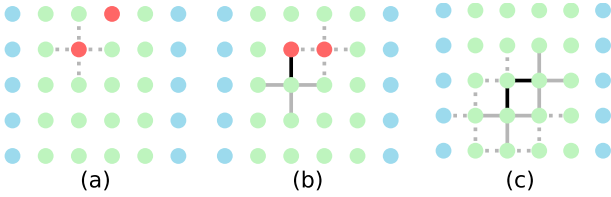


Figure 4: A concrete depiction of Fig. 3b for a distance-5 code to show how the 1:1 cluster growth schedule violates Lemma 2. Ungrown edges are invisible; half-grown, dotted; fully grown, solid. Edges bitflipped by the decoder are in black.

or one defect will remain, indicating the defect count parity.

To ‘push a defect’ we simply bitflip the edge we want to push it along (this is consistent with Definition 1 and with the previous paragraph: if there is a defect at the other end of the edge, they annihilate). This way, \mathbb{T} is the symmetric difference of all the paths traced by defects and moreover is guaranteed to be complete within any inactive cluster. The idea then is to inactivate all clusters once they have fallen far enough.

4.1 Cluster Growth Schedules

In this paper we consider two different *cluster growth schedules* i.e. rules on how active clusters grow. Section 4.1.1 introduces the simplest possible one, 1:1, and identifies an issue that hinders its accuracy. We

fix this in Section 4.1.2 with an improved schedule, 2:1.

4.1.1 1:1 Schedule

In the most straightforward schedule, Snowflake performs one growth round per decoding cycle, as the example in Fig. 4 shows. A *growth round* here comprises growing each active cluster in all possible (defined by the edges of G) directions by half an edge, merging touching clusters and pushing defects to roots. Algorithm 1 summarises this.

Algorithm 1 Snowflake with the 1:1 schedule.

```

raise  $W$ 
grow all active clusters by  $\frac{1}{2}$ 
MERGE

procedure MERGE
┌   merge touching clusters
└   push defects to roots

```

To see the issue with this schedule, first note the following lemma for [29, Theorem 1] that is satisfied by original UF.

Lemma 2. *Whenever a cluster grows, the number of bitflipped edges covered by the union of all clusters increases by $\geq 1/2$.*

The theorem leads to the following for original UF.

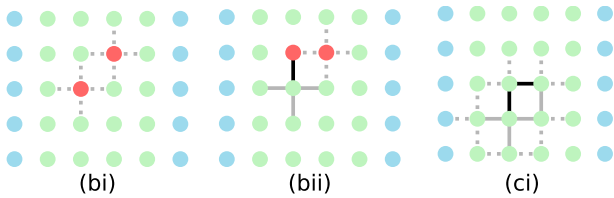


Figure 5: Continuing from Fig. 4a but with the 2:1 cluster growth schedule, which shows Lemma 2 is no longer violated. ‘i’ labels the first growth round of the decoding cycle; ‘ii’, the second.

Corollary 1. *Any combination of $s < d/2$ bitflips can be corrected.*

Proof. Lemma 2 guarantees that after $2s$ growth rounds, all bitflipped edges are covered by the union of all clusters, and no more growth occurs. The largest possible cluster diameter after this many growth rounds is $2s < d$ so no logical bitflip is possible. \square

For Snowflake with the 1:1 schedule, it is possible for two active clusters to be only half an edge apart; see e.g. Fig. 4b. Then, during growth, they will overgrow ‘into each other’ rather than stop growing as soon they touch. This violates Lemma 2 and leads to unnecessarily large clusters. E.g. assume the defect pair in Fig. 4a resulted from $s = 2$ bitflipped edges; in c, two clusters grow but only $1/2$ more of the bitflipped edges are covered. The resultant cluster has diameter $9/2 > s$.

4.1.2 2:1 Schedule

To fix this, we can grow clusters more cautiously. Note in Fig. 4b it is enough for just one of the clusters to grow for the two to merge, and the reason they are half an edge apart is that one has grown an even, and the other an odd, number of times. So, define a *whole (half) cluster* as one that has grown an even (odd) number of times, and a *mixed cluster* as one that has resulted from merging a whole with a half cluster. Visually, a whole (half) cluster is, when isolated (always), surrounded by ungrown (half-grown) edges. A mixed cluster, e.g. in Fig. 4c, is always surrounded by both types of edge.

In this schedule, Snowflake performs two different growth rounds per decoding cycle: first growing the whole clusters, then the half clusters, as Fig. 5 shows. After each round, all clusters reevaluate their activity. Mixed clusters need not be considered due to the following.

Proposition 1. *Mixed clusters never occur with the 2:1 schedule.*

We prove this in Appendix B. Lastly, for balance, whole clusters that grow in the first round (thus becoming half clusters) do not grow again in the same decoding cycle. Algorithm 2 summarises this.

Algorithm 2 Snowflake with the 2:1 schedule.

```

raise  $W$ 
2: grow all active whole clusters by  $\frac{1}{2}$ 
MERGE
4: for all active half clusters  $C$  do
   if no part of  $C$  grew in Line 2 then
6:    $\lfloor \lfloor$  grow  $C$  by  $\frac{1}{2}$ 
MERGE

```

The 2:1 schedule satisfies Lemma 2 as it prevents the overgrowth issue: if two active clusters are half an edge apart, only one of them will grow. E.g. in Fig. 5ci, only the whole cluster (lower west) grows and the resultant half cluster has diameter $4 = 2s$. Our numerics in Appendix C show the 2:1 schedule almost doubles the threshold of 1:1, so for the rest of this paper, we consider Snowflake with the 2:1 schedule.

4.2 Constructing the Viewing Window

Even despite Remark 1 we define $W = (V_W, E_W)$ sans temporal boundary because in either schedule, clusters fall twice as fast as they grow so this boundary would never be touched.

The height of the buffer region is lower-bounded by the following.

Proposition 2. *The minimum layer count of the buffer region that guarantees Condition 1, is $b_{\min} := 2\lfloor d/2 \rfloor$.*

Proof. Defects are annihilated by either meeting another defect or being pushed to a boundary. So a longest-living defect is one like that in Fig. 3a: never meeting another defect, and created as far as possible, i.e. $\lfloor d/2 \rfloor$ edges, from any boundary. The cluster containing this defect grows outward by half an edge per decoding cycle so will touch a boundary after b_{\min} decoding cycles, at the $(b_{\min} + 1)^{\text{th}}$ layer from the top. So \mathbb{T} is always complete in this layer and below, but not above. \square

We set $b = b_{\min}$ for our local implementation. Minimising c and b in the frugal method roughly halves the height of W compared to the forward method for $c = b = d$. This halves the processor count of our implementation described in the next subsection.

4.3 Local Implementation

We use the same local architecture of Macar and Actis in [14] i.e. a processor for each node in V_W , a communication link for each edge and one controller which manages the global variables of the algorithm. For the surface code, the processors and links form a 3D lattice oriented so the time axis points upward, as in Fig. 5 but with an extra spatial dimension.

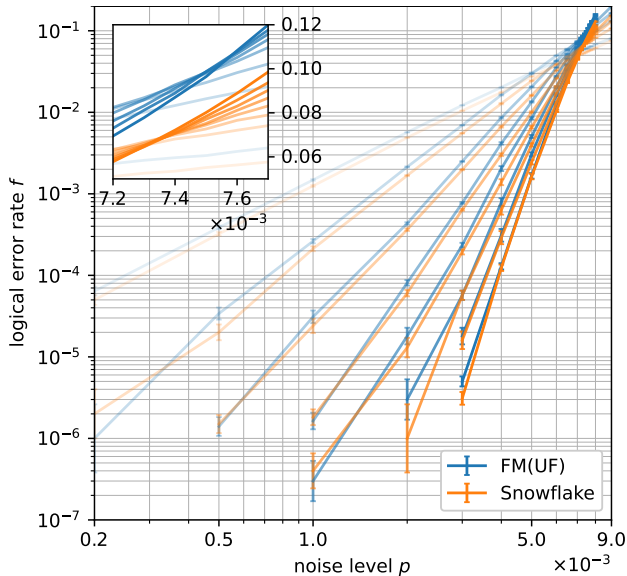


Figure 6: Threshold plots for the surface code under circuit-level noise. Each line corresponds to a fixed distance $d = 3, 5, \dots, 17$ from shallowest to steepest. Each datapoint is the mean of 10^4 – 10^7 lots of d measurement rounds; errorbars show standard error. The inset zooms in on both thresholds whose coordinate $(p, f)_{\text{th}}$ is around $(0.755, 10.5) \cdot 10^{-2}$ for UF adapted with the forward method, and $(0.735, 6.8) \cdot 10^{-2}$ for Snowflake. Here, the standard error is smaller than the line thickness.

Snowflake is compatible with any choice of network for controller–processor communication, be it the hierarchical tree used in Macar or the strictly local staging and signalling tree in Actis, with synchronous or asynchronous logic. We thus leave this as an implementation choice.

Our implementation follows discrete timesteps with each component performing one operation, and messages travelling one link, per timestep. Loosely speaking, it is a pipelined decoder as successively lower layers in the lattice process increasingly mature stages of decoding. Appendix D provides the rest of the details.

5 Numerics

We wrote a Python package [38] to emulate our local implementation of Snowflake. We use it to run the memory experiment (preserving a logical qubit) using the surface code under the circuit-level noise model detailed in [14, §B]. Specifically, we decode the syndrome from $n \gg d$ measurement rounds, then count one of two features depending on if we are benchmarking accuracy or runtime.

For comparison we also benchmark FM(UF). We fix its viewing window to $c = b = d$ as we found that smaller c, b values led to both worse accuracies and overall runtimes.

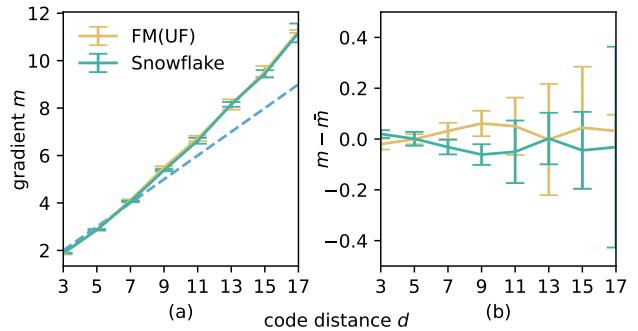


Figure 7: Errorbars show standard error. (a) Gradient of the lines in the $p \leq 6 \cdot 10^{-3}$ region of Fig. 6, estimated using Weighted Least Squares. The dashed blue line shows the asymptotic ($p \rightarrow 0$) value $m = (d + 1)/2$ from theory [49, §5]. (b) Deviation of said gradient from the mean $\bar{m} := \frac{1}{2}(m_{\text{FM(UF)}} + m_{\text{Snowflake}})$ of both decoders.

5.1 Accuracy

For this we count the number l of logical bitflips in the leftover. We identify these paths between opposite boundaries using the method described in [50]. We then estimate the logical error rate $\hat{f} = ld/n$ as per Definition 2.

Figure 6 compares the accuracy of FM(UF) and Snowflake, for practical noise levels and code distances. Below threshold, we assume the power law $f/f_{\text{th}} = (p/p_{\text{th}})^m$. Figure 7 shows the subthreshold gradients $m(d)$ are indistinguishable for the two decoders so we can characterise their accuracy difference solely by their thresholds.

While FM(UF) has a slightly higher threshold, Snowflake leads to a logical qubit lifetime $1/f$ that is 24.9(5)% longer on average over the Fig. 6 data. We are unsure why Snowflake is more accurate but suspect it may relate to its smoother treatment of G . The most obvious difference between the outputs of UF and Snowflake is in the relative cluster sizes e.g. were UF used in Fig. 5, both clusters would be the same size when they merge.

5.2 Runtime

For this we count the number of timesteps to decode. We consider this per d measurement rounds as each logical operation lasts $\mathcal{O}(d)$ rounds using lattice surgery [51], the best known technique for universal computation with the surface code when the quantum device has local connectivity [52, 53]. We also consider the timestep count *per measurement round* because for real-time decoding, the decoder’s throughput requirement is imposed by the quantum device’s stabiliser cycle duration [16, §1] e.g. $\approx 1 \mu\text{s}$ for superconducting qubits [54, Figure 1] [55, §V].

Figure 8 compares the runtime of FM(Macar) and Snowflake. We exclude their controller–processor communication cost by assuming implementations where the controller connects directly to each pro-

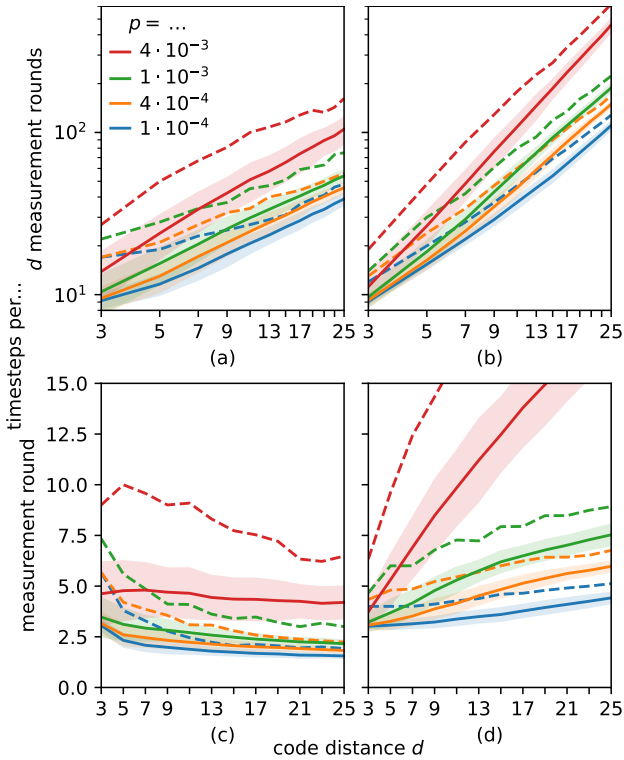


Figure 8: Decoder runtime against surface code distance d , for various circuit-level noise levels p below threshold. Each solid (dashed) line shows the mean (99th percentile) of 10^3 lots of d measurement rounds; shading shows standard deviation. The standard error of the mean is smaller than the solid line thickness. (a) Macar [14] adapted with the forward method. (b) Snowflake. (c) Same as ab but rescaled. (d) Same as ab but rescaled.

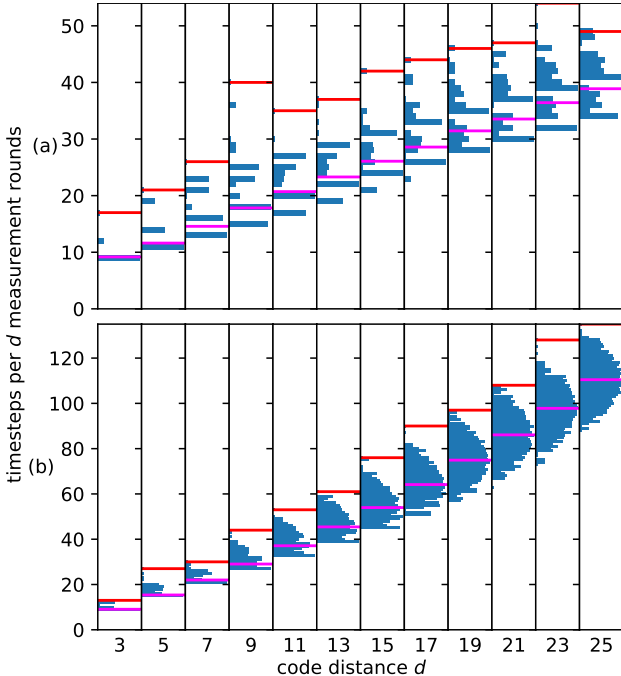


Figure 9: A more detailed view of the $p = 10^{-4}$ data in Fig. 8a and b, respectively. Within each histogram: the horizontal magenta (red) line shows the mean (maximum) of 10^3 lots of d measurement rounds, the x -axis scale is logarithmic, and each bar has width 1.

cessor. To adapt Macar with the forward method, we measure its runtime to decode a viewing window, then add c timesteps due to [step 3](#) of the forward method. Using this data, [Table 1](#) estimates the scaling m , assuming mean runtime $\propto d^m$. FM(Macar)’s scaling is sublinear whereas Snowflake’s is subquadratic.

Table 1: Gradient m of the solid lines in [Fig. 8ab](#) estimated using Weighted Least Squares.

p	FM(Macar)	Snowflake
$4 \cdot 10^{-3}$	0.94(1)	1.770(4)
10^{-3}	0.778(8)	1.42(1)
$4 \cdot 10^{-4}$	0.761(7)	1.34(2)
10^{-4}	0.69(2)	1.16(2)

Remark 2. We suspect that this is because for FM(Macar), active clusters in the same batch all grow at the same time regardless of their vertical coordinate. In Snowflake, this process is somewhat serialised: older active clusters start growing before newer ones do, as they enter W earlier; see e.g. [Fig. 3b](#).

Despite this discrepancy, subquadratic is still better than the slightly-higher-than-cubic scaling [[56](#), §2.3] of original UF.

To investigate the practical regime further, [Fig. 9](#) plots the distribution of runtimes for both decoders at the lowest emulated noise level, where Snowflake is ≈ 2 – 3 times slower than FM(Macar). Neither distribution has a long tail; such consistent runtimes are beneficial for hard real-time decoding: the time limit can be set lower for a given target timeout failure rate, accelerating the quantum program and increasing qubit coherence.

6 Conclusion

We propose the frugal method for stream decoding of quantum error-correcting codes for which there exists a decoding graph embeddable in \mathbb{R}^3 without ‘long-range’ edges. As [[42](#), §V] points out, this paradigm of reusing decoder information from previous windows has been explored already for *classical* LDPC codes e.g. in [[57](#), §III.B.2]. We also design Snowflake, a simple decoder compatible with the frugal method and numerically benchmark its local implementation. It is more accurate than original UF and its runtime scales better. There are various avenues of further investigation for the frugal method and Snowflake:

2D Architecture The serialisation in the vertical direction mentioned in [Remark 2](#) suggests the viability of an alternative architecture: ‘flattening’ the 3D lattice down onto a 2D grid so there is one processor for each *set of nodes* of the same (x, y) coordinate i.e. each ancilla qubit. This comes at the cost of serialising the operations within each set, but if these opera-

tions are inherently serial, the cost could be marginal. There are two benefits: first, it is more practical as a 2D chip is far easier to build than a 3D lattice of processors; second, messages passed vertically would be instantaneous within a timestep. Future work would involve emulation and numerical analysis of this flattened implementation.

Asynchronous Logic As discussed in [14, §6], controller–processor communication could run by asynchronous (instead of synchronous) logic, which would speed up Snowflake. One could explore which other processes in Snowflake could be sped up by asynchronous logic.

Weighted Edges Clusters could grow along edges at different speeds to account for their different bit-flip probabilities, which would improve accuracy [18]. These speeds could even be configurable in the hardware to fine-tune the noise model during a calibration stage; this however would alter [Proposition 2](#), requiring b_{\min} to also be configurable, which is nontrivial.

Computation Recently, the sandwich method has been generalised from quantum memory to lattice surgery-based computation [44, 45, 58]. We propose an alternative approach to decoding lattice surgery that exploits the granular and local nature of Snowflake. Imagine the decoder as a homogeneous substrate positioned just above the entire 2D lattice of qubits. Regions of this substrate are turned on (to decode) wherever the below qubits are involved in surgery. Snowflake would work best with so-called *twist-free* lattice surgery [59, §IV] which minimises the use of nonlocal stabilisers. These elongated stabilisers introduce in G additional detectors [60, Appendix A.3] and accounting for them in our scheme would be nontrivial. Some details of the local implementation in [Appendix D.1](#) would need to be generalised. E.g. since boundaries vary during lattice surgery, the ID of each processor would no longer be a constant integer; rather, a combination of a constant 3D coordinate and a (relative) variable boolean indicating whether the processor represents a boundary node. This preserves [Remark 3](#). For controller–processor communication, a hierarchical tree like that used in Macar would be best, as communication cost would then scale logarithmically with the length of the qubit lattice, which may be much larger than d .

Acknowledgments

I thank Simon Benjamin, Matt Cassie, and Armands Strikis for useful discussions, and Alexandru Paler and Timo Hillmann for helpful comments. I acknowledge the use of the University of Oxford Advanced

Research Computing (ARC) facility [61] in carrying out this work and specifically the facilities made available from the EPSRC QCS Hub grant (agreement No. EP/T001062/1). I also acknowledge support from an EPSRC DTP studentship and two EPSRC projects: RoaRQ (EP/W032635/1) and SEEQA (EP/Y004655/1). Open-source Python libraries used in this work include `matplotlib`, `networkx`, `numpy`, `pandas`, `pytest`, `scipy`, `statsmodels`.

Competing Interests

The author declares a relevant patent application: UK patent application number GB2418283.4.

References

- [1] D. J. Reilly. “Challenges in scaling-up the control interface of a quantum computer”. In 2019 IEEE International Electron Devices Meeting (IEDM). [Pages 31.7.1–31.7.6](#). (2019).
- [2] Poulami Das, Christopher A. Pattison, Srilatha Manne, Douglas M. Carmean, Krysta M. Svore, Moinuddin Qureshi, and Nicolas Delfosse. “AFS: Accurate, fast, and scalable error-decoding for fault-tolerant quantum computers”. In 2022 IEEE International Symposium on High-Performance Computer Architecture (HPCA). [Pages 259–273](#). (2022).
- [3] Nicolas Delfosse, Andres Paz, Alexander Vaschillo, and Krysta M. Svore. “How to choose a decoder for a fault-tolerant quantum computer? the speed vs accuracy trade-off” (2023). [arXiv:2310.15313](#).
- [4] James William Harrington. “Analysis of quantum error-correcting codes: symplectic lattice codes and toric codes”. [PhD thesis](#). California Institute of Technology. (2004).
- [5] Austin G. Fowler. “Minimum weight perfect matching of fault-tolerant topological quantum error correction in average $O(1)$ parallel time” (2014). [arXiv:1307.1740](#).
- [6] Michael Herold, Earl T. Campbell, Jens Eisert, and Michael J. Kastoryano. “Cellular-automaton decoders for topological quantum memories”. [npj Quantum Information 1, 15010](#) (2015).
- [7] Nikolas P. Breuckmann, Kasper Duivenvoorden, Dominik Michels, and Barbara M. Terhal. “Local decoders for the 2D and 4D toric code” (2016). [arXiv:1609.00510](#).
- [8] Michael Herold, Michael J. Kastoryano, Earl T. Campbell, and Jens Eisert. “Cellular automaton decoders of topological quantum memories in the fault tolerant setting”. [New Journal of Physics 19, 063012](#) (2017).
- [9] Nicolai Lang and Hans Peter Büchler. “Strictly local one-dimensional topological quantum er-

- ror correction with symmetry-constrained cellular automata”. *SciPost Physics* **4**, 007 (2018).
- [10] Aleksander Kubica and John Preskill. “Cellular-automaton decoders with provable thresholds for topological codes”. *Physical Review Letters* **123**, 020501 (2019).
- [11] Nicolas Delfosse. “Hierarchical decoding to reduce hardware requirements for quantum computing” (2020). [arXiv:2001.11427](https://arxiv.org/abs/2001.11427).
- [12] Samuel C. Smith, Benjamin J. Brown, and Stephen D. Bartlett. “Local predecoder to reduce the bandwidth and latency of quantum error correction”. *Physical Review Applied* **19**, 034050 (2023).
- [13] Barbara M. Terhal. “Quantum error correction for quantum memories”. *Review of Modern Physics* **87**, 307–346 (2015).
- [14] Tim Chan and Simon C. Benjamin. “Actis: A strictly local Union-Find decoder”. *Quantum* **7**, 1183 (2023).
- [15] L. M. K. Vandersypen, H. Bluhm, J. S. Clarke, A. S. Dzurak, R. Ishihara, A. Morello, D. J. Reilly, L. R. Schreiber, and M. Veldhorst. “Interfacing spin qubits in quantum dots and donors—hot, dense, and coherent”. *npj Quantum Information* **3**, 34 (2017).
- [16] Francesco Battistel, Christopher Chamberland, Kauser Johar, Ramon W. J. Overwater, Fabio Sebastiano, Luka Skoric, Yosuke Ueno, and Muhammad Usman. “Real-time decoding for fault-tolerant quantum computing: progress, challenges and outlook”. *Nano Futures* **7**, 032003 (2023).
- [17] Muyuan Li, Daniel Miller, Michael Newman, Yukai Wu, and Kenneth R. Brown. “2D compass codes”. *Physical Review X* **9**, 021041 (2019).
- [18] Shilin Huang, Michael Newman, and Kenneth R. Brown. “Fault-tolerant weighted union-find decoding on the toric code”. *Physical Review A* **102**, 012419 (2020).
- [19] Shui Hu. “Quasilinear time decoding algorithm for topological codes with high error threshold”. *Master’s thesis*. Delft University of Technology. (2020).
- [20] Nicolas Delfosse and Matthew B. Hastings. “Union-find decoders for homological product codes”. *Quantum* **5**, 406 (2021).
- [21] Christopher A. Pattison, Michael E. Beverland, Marcus P. da Silva, and Nicolas Delfosse. “Improved quantum error correction using soft information” (2021). [arXiv:2107.13589](https://arxiv.org/abs/2107.13589).
- [22] Nicolas Delfosse, Vivien Londe, and Michael E. Beverland. “Toward a union-find decoder for quantum LDPC codes”. *IEEE Transactions on Information Theory* **68**, 3187–3199 (2022).
- [23] Lucas Berent, Lukas Burgholzer, and Robert Wille. “Software tools for decoding quantum low-density parity-check codes”. In Proceedings of the 28th Asia and South Pacific Design Automation Conference. Pages 709–714. ASPDAC ’23 New York, NY, USA (2023). Association for Computing Machinery.
- [24] Ben Barber, Kenton M. Barnes, Tomasz Bialas, Okan Buğdaycı Earl T. Campbell, Neil I. Gillespie, Kauser Johar, Ram Rajan, Adam W. Richardson, Luka Skoric, Canberk Topal, Mark L. Turner, and Abbas B. Ziad. “A real-time, scalable, fast and highly resource efficient decoder for a quantum computer” (2023). [arXiv:2309.05558](https://arxiv.org/abs/2309.05558).
- [25] Sam J. Griffiths and Dan E. Browne. “Union-find quantum decoding without union-find”. *Physical Review Research* **6**, 013154 (2024).
- [26] Matthias C. Löbl, Susan X. Chen, Stefano Paesani, and Anders S. Sørensen. “Breadth-first graph traversal union-find decoder” (2024). [arXiv:2407.15988](https://arxiv.org/abs/2407.15988).
- [27] Nadine Meister, Christopher A. Pattison, and John Preskill. “Efficient soft-output decoders for the surface code” (2024). [arXiv:2405.07433](https://arxiv.org/abs/2405.07433).
- [28] Nicolas Delfosse and Gilles Zémor. “Linear-time maximum likelihood decoding of surface codes over the quantum erasure channel”. *Physical Review Research* **2**, 033042 (2020).
- [29] Nicolas Delfosse and Naomi H. Nickerson. “Almost-linear time decoding algorithm for topological codes”. *Quantum* **5**, 595 (2021).
- [30] Namitha Liyanage, Yue Wu, Siona Tagare, and Lin Zhong. “FPGA-based distributed union-find decoder for surface codes”. *IEEE Transactions on Quantum Engineering* **5**, 1–18 (2024).
- [31] Maximilian Jakob Heer, Emanuele Del Sozzo, Keisuke Fujii, and Kentaro Sano. “Novel union-find-based decoders for scalable quantum error correction on systolic arrays”. In 2023 IEEE International Parallel and Distributed Processing Symposium Workshops (IPDPSW). Pages 524–533. (2023).
- [32] Maximilian Jakob Heer, Jan-Erik R. Wichmann, and Kentaro Sano. “Achieving scalable quantum error correction with union-find on systolic arrays by using multi-context processing elements”. In 2023 IEEE International Conference on Quantum Computing and Engineering (QCE). Volume 02, pages 242–243. (2023).
- [33] Abbas B. Ziad, Ankit Zalawadiya, Canberk Topal, Joan Camps, György P. Gehér, Matthew P. Stafford, and Mark L. Turner. “Local clustering decoder: a fast and adaptive hardware decoder for the surface code” (2024). [arXiv:2411.10343](https://arxiv.org/abs/2411.10343).
- [34] Namitha Liyanage, Yue Wu, Alexander Deters, and Lin Zhong. “Scalable quantum error correction for surface codes using FPGA”. In 2023 IEEE International Conference on Quan-

- tum Computing and Engineering (QCE). **Volume 01, pages 916–927**. (2023).
- [35] Eric Dennis, Alexei Kitaev, Andrew Landahl, and John Preskill. “Topological quantum memory”. *Journal of Mathematical Physics* **43**, 4452–4505 (2002).
- [36] Luka Skoric, Dan E. Browne, Kenton M. Barnes, Neil I. Gillespie, and Earl T. Campbell. “Parallel window decoding enables scalable fault tolerant quantum computation”. *Nature Communications* **14**, 7040 (2023).
- [37] Xinyu Tan, Fang Zhang, Rui Chao, Yaoyun Shi, and Jianxin Chen. “Scalable surface-code decoders with parallelization in time”. *PRX Quantum* **4**, 040344 (2023).
- [38] Tim Chan (2023). code: [timchan0/localuf](#).
- [39] Ashley M. Stephens. “Fault-tolerant thresholds for quantum error correction with the surface code”. *Physical Review A* **89**, 022321 (2014).
- [40] Lucas Berent, Timo Hillmann, Jens Eisert, Robert Wille, and Joschka Roffe. “Analog information decoding of bosonic quantum low-density parity-check codes”. *PRX Quantum* **5**, 020349 (2024).
- [41] Shilin Huang and Shruti Puri. “Increasing memory lifetime of quantum low-density parity check codes with sliding-window noisy syndrome decoding”. *Physical Review A* **110**, 012453 (2024).
- [42] Anqi Gong, Sebastian Cammerer, and Joseph M. Renes. “Toward low-latency iterative decoding of QLDPC codes under circuit-level noise” (2024). [arXiv:2403.18901](#).
- [43] Kao-Yueh Kuo and Ching-Yi Lai. “Fault-tolerant belief propagation for practical quantum memory” (2024). [arXiv:2409.18689](#).
- [44] Héctor Bombín, Chris Dawson, Ye-Hua Liu, Naomi Nickerson, Fernando Pastawski, and Sam Roberts. “Modular decoding: parallelizable real-time decoding for quantum computers” (2023). [arXiv:2303.04846](#).
- [45] Sophia Fuhui Lin, Eric C. Peterson, Krishanu Sankar, and Prasahnt Sivarajah. “Spatially parallel decoding for multi-qubit lattice surgery” (2024). [arXiv:2403.01353](#).
- [46] Poulami Das, Aditya Locharla, and Cody Jones. “LILLIPUT: a lightweight low-latency lookuptable decoder for near-term quantum error correction”. In Proceedings of the 27th ACM International Conference on Architectural Support for Programming Languages and Operating Systems. **Pages 541–553**. New York, NY, USA (2022). Association for Computing Machinery.
- [47] Emanuel Knill. “Quantum computing with realistically noisy devices”. *Nature* **434**, 39–44 (2005).
- [48] L. Rieseboos, X. Fu, S. Varsamopoulos, C. G. Almuvever, and K. Bertels. “Pauli frames for quantum computer architectures”. In Proceedings of the 54th Annual Design Automation Conference 2017. **Pages 1–6**. New York, NY, USA (2017). Association for Computing Machinery.
- [49] Austin G. Fowler, Adam C. Whiteside, and Lloyd C. L. Hollenberg. “Towards practical classical processing for the surface code: Timing analysis”. *Physical Review A* **86**, 042313 (2012).
- [50] Tim Chan. “Benchmarking accuracy in an emulated memory experiment” (2024). [arXiv:2411.02505](#).
- [51] Dominic Horsman, Austin G. Fowler, Simon Devitt, and Rodney Van Meter. “Surface code quantum computing by lattice surgery”. *New Journal of Physics* **14**, 123011 (2012).
- [52] Austin G. Fowler and Craig Gidney. “Low overhead quantum computation using lattice surgery” (2019). [arXiv:1808.06709](#).
- [53] Daniel Litinski. “A game of surface codes: Large-scale quantum computing with lattice surgery”. *Quantum* **3**, 128 (2019).
- [54] Google Quantum AI. “Suppressing quantum errors by scaling a surface code logical qubit”. *Nature* **614**, 676–681 (2023).
- [55] Google Quantum AI and Collaborators. “Quantum error correction below the surface code threshold” (2024). [arXiv:2408.13687](#).
- [56] Namitha Liyanage, Yue Wu, Alexander Deters, and Lin Zhong. “Scalable quantum error correction for surface codes using FPGA” (2023). [arXiv:2301.08419](#).
- [57] Inayat Ali, Jong-Hwan Kim, Sang-Hyo Kim, Heeyoul Kwak, and Jong-Seon No. “Improving windowed decoding of SC LDPC codes by effective decoding termination, message reuse, and amplification”. *IEEE Access* **6**, 9336–9346 (2018).
- [58] Craig Gidney. “Stability experiments: The overlooked dual of memory experiments”. *Quantum* **6**, 786 (2022).
- [59] Christopher Chamberland and Earl T. Campbell. “Universal quantum computing with twist-free and temporally encoded lattice surgery”. *PRX Quantum* **3**, 010331 (2022).
- [60] György P. Gehér, Ophelia Crawford, and Earl T. Campbell. “Tangling schedules eases hardware connectivity requirements for quantum error correction”. *PRX Quantum* **5**, 010348 (2024).
- [61] Andrew Richards. “University of Oxford Advanced Research Computing”. (2015).

A What the Decoding Graph Represents

Since the stream decoding problem is defined for only phenomenological and circuit-level noise, we explain what G physically represents under these two models.

Each detector represents the difference between two consecutive measurements of an ancilla qubit at a given point in time. Boundary nodes represent nothing physical.

There are two types of edges: bulk edges, which are not incident to a boundary node, and boundary edges, which are. Each bulk (boundary) edge represents a possible pair of defects (a possible defect) that could have resulted from one fault. A *fault* is defined for phenomenological noise as either a data qubit bitflip or a measurement outcome flip; for circuit-level noise, an error process in the syndrome extraction circuit.

Note G allows for correcting only bitflips i.e. \hat{X} errors. The full decoding problem in practice requires another similar-looking but independent decoding graph (with its own separate decoder) to allow for correcting phaseflips i.e. \hat{Z} errors.

B Proof of Proposition 1

We first define three functions. The *wholeness* of a non-mixed cluster C is

$$\text{wh } C := \begin{cases} 1 & C \text{ a whole cluster,} \\ \frac{1}{2} & C \text{ a half cluster.} \end{cases} \quad (1)$$

The *ungrown length* of a path P in W that comprises f fully grown edges, h half-grown edges, and z un-grown edges, is

$$l(P) := \frac{1}{2}h + z. \quad (2)$$

The *ungrown distance* between clusters C, D is the minimum un-grown length of a path from a node in C to a node in D :

$$d(C, D) := \min\{l(uv, \dots, wx) : ux \in V_C \times V_D\}. \quad (3)$$

Now consider the following.

Lemma 3. *After each growth round of Snowflake with the 2:1 schedule, we have*

$$d(C, D) \in \mathbb{Z} + \text{wh } C + \text{wh } D \quad (4)$$

for any two non-mixed clusters C, D .

Proof. By induction on the number r of growth rounds elapsed.

Consider base case $r = 0$. All edges in W are un-grown so $l(P) \in \mathbb{Z}$ for any path P in W , and so $d(C, D) \in \mathbb{Z}$. All clusters are whole so $\text{wh } C + \text{wh } D = 2$, and so Eq. (4) true for $r = 0$.

Now the inductive step; assume true after r growth rounds and consider growth round $r + 1$. If...

1. neither C nor D grows, all terms in Eq. (4) are unchanged;
2. C grows but not D , $d(C, D)$ decreases by $\frac{1}{2}$ and $\text{wh } C$ changes by $\frac{1}{2}$;

3. both C and D grow, we must have $\text{wh } C + \text{wh } D \in \{1, 2\}$, so C and D cannot be half an edge apart before growth, so $d(C, D)$ decreases by 1. Also, $\text{wh } C$ and $\text{wh } D$ each change by $\frac{1}{2}$.

In each case, Eq. (4) remains true. \square

Now we can prove the desired statement.

Proof of Proposition 1. There are no mixed clusters initially. By Lemma 3, a whole cluster never merges with a half cluster, so mixed clusters never form. \square

C Schedule Accuracy Comparison

Section 4.1 discussed 1:1 and 2:1 as two possible cluster growth schedules for Snowflake. Figure 10 shows how Snowflake performs with each schedule: 2:1 almost doubles the threshold p_{th} of 1:1.

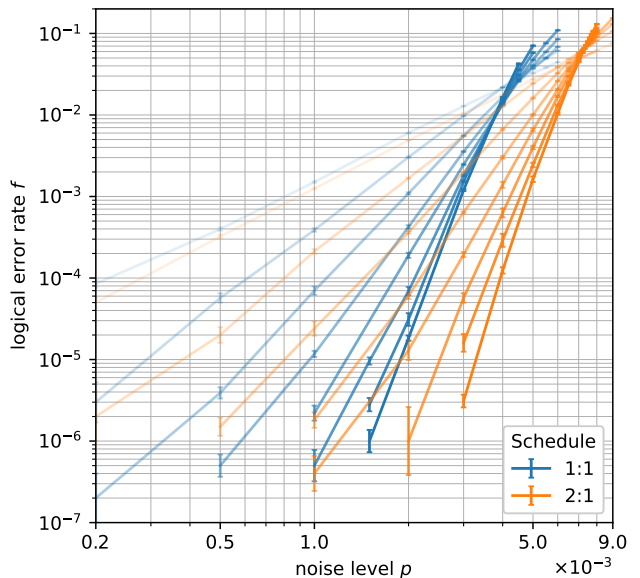


Figure 10: Same as Fig. 6 but the blue lines instead show data for Snowflake with the 1:1 cluster growth schedule. The coordinate $(p, f)_{\text{th}}$ of the threshold is around $(0.375, 9) \cdot 10^{-2}$ for 1:1, and $(0.735, 6.8) \cdot 10^{-2}$ for 2:1.

D Local Implementation of Snowflake

In this section we refer to processors as nodes and communication links as edges. The controller can broadcast the same boolean to, and receive (without knowing the sender) booleans from, every node.

In Appendix D.1 we list the variables each component stores and in Appendix D.2 we explain how they are manipulated in order to effect Snowflake. Appendices D.3 and D.4 explain the variable-duration stages in more detail.

D.1 Setup

Each node $v \in V_W$ is assigned a unique integer ID and stores the following variables:

1. **active** is a boolean indicating whether v is in an active cluster. If $v.\text{active} = \text{true}$ we say v is active.
2. **whole** is a boolean indicating whether v is in a whole cluster. If $v.\text{whole} = \text{true}$ we say v is whole.
3. **CID** is an integer indicating the cluster that v belongs to. Clusters are identified by the lowest ID of all its nodes. The node of this ID is the root. CID can also adopt the value **reset** to indicate v should *unroot* (defined in [Appendix D.4.2](#)) in the next timestep.
4. **defect** is a boolean indicating whether v has a defect. This can be thought of as a particle which is passed between nodes. When a node receives two defects in a timestep, they annihilate.
5. **pointer** is the direction v should push the defect (by bitflipping the corresponding edge). Possible values (under circuit-level noise) are C, N, W, E, S, D, U, NU, WD, EU, SD, NWD, SEU, representing respectively centre, north, west, east, south, down, up, and combinations thereof. Following the pointers starting from v should eventually lead to the root of the cluster that v is in. Only roots have **pointer** = C as they do not push defects but accumulate them.
6. **grown** is a boolean indicating whether the cluster that v is in has grown in the first growth round of the current decoding cycle.
7. **unrooted** is a boolean indicating whether v has unrooted in the current decoding cycle.
8. **busy** is a boolean indicating whether v is busy.
9. **stage** is the current stage of Snowflake. This follows the flowchart in [Fig. 11](#).

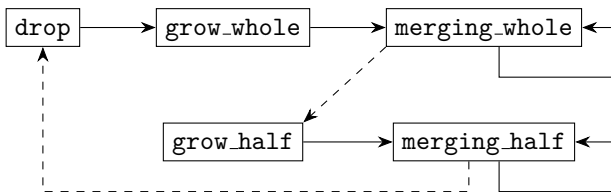


Figure 11: Flowchart for the stages of Snowflake: **drop**, **grow_whole**, and **grow_half** each last one timestep whereas the other two last a variable number, hence their loops. The dashed (solid) arrows indicate advances by the global controller (each node locally). Snowflake cycles through all five stages once per decoding cycle.

We refer to the first five variables as *relative* and the last four as *absolute*. Each edge $e \in E_W$ has the following variables:

1. **growth** is its growth value which is in $\{0, \frac{1}{2}, 1\}$. Two clusters touch when they become connected via a fully grown edge.
2. **correction** is a boolean indicating if $e \in \mathbb{T}$.

These are stored as additional relative variables at the endpoint with the lower ID. It helps to define the *owned edges* as those whose variables a node stores:

$$v.\text{owned} := \{uv : uv \in E_W \text{ and } v.\text{ID} < u.\text{ID}\}. \quad (5)$$

D.2 Procedures

Though the pseudocode in this subsection explains exactly what each component does, it is difficult to infer from this the *emergent effect*. We describe the latter in the accompanying prose.

Algorithm 3 Run by controller every timestep.

```

if not (waiting or any  $v.\text{busy}$ ) then
  for all  $v \in V_W$  do
     $v.\text{stage} \leftarrow$  next stage
    if  $v.\text{stage}$  was merging_whole then
      wait 1 timestep
    else  $\triangleright v.\text{stage}$  was merging_half
      wait 2 timesteps
  
```

In each timestep the controller runs [Algorithm 3](#) which, during either merging stage, tells all nodes to advance to the next stage if none of them are busy. This is the only time the controller needs to communicate with the nodes, as the merging stages are the only ones of variable duration.

Algorithm 4 Run by node v every timestep.

```

call the procedure in Algorithm 5 matching  $v.\text{stage}$ 
if  $v.\text{stage} \neq$  merging then
   $v.\text{stage} \leftarrow$  next stage
  
```

At the same time, each node v runs [Algorithm 4](#), calling procedures from [Algorithm 5](#). Stage **drop** adds to C and raises W by one layer, as in [Fig. 12b](#). Each node v in the top sheet of W starts in its own cluster, thus sets its relative variables to reflect this ([Lines 10 and 11](#)). $v.\text{whole}$, $v.\text{CID}$, and $v.\text{pointer}$ need not be explicitly reset as they never change from their correct values of **true**, $v.\text{ID}$, and C, respectively.

Stage **grow_whole** grows all edges around each active whole cluster by $\frac{1}{2}$, as in [Fig. 12c](#). Stage **grow_half** does the same but for active half clusters that have not already grown in the current decoding cycle, as in [Fig. 12e](#).

[Figure 12d](#) shows a merging example that lasts just one timestep, and [f-h](#) shows one that needs three

Algorithm 5 The five procedures that can be called in [Algorithm 4](#).

```

procedure DROP( $v$ )
2:    $v.grown \leftarrow \text{false}$ 
   for  $e \in v.owned \cap \text{commit region}$  do
4:     if  $e.correction$  then  $\triangleright$  Commit  $e$ .
        $C \leftarrow C \Delta \{e\}$ 
6:     if  $\exists$  node  $u$  below  $v$  then  $\triangleright$  Shift relative data down one layer.
        $v.CID \leftarrow \text{ID of node below current root}$ 
8:     send all relative variables to  $u$ 
       if  $v \in \text{top sheet of } W$  then  $\triangleright$  Inherit the new measurement round results.
10:     $v.defect \leftarrow \text{whether the measurement of the corresponding ancilla qubit differs from the last round}$ 
     $v.active \leftarrow \text{false}$ 
12:
procedure GROWWHOLE( $v$ )
14:  if  $v.active$  and  $v.whole$  then
    GROW( $v$ )
16:   $v.grown \leftarrow \text{true}$ 
    if  $v \in \text{bottom sheet of } W$  and  $v.pointer \ni D$  then  $\triangleright$  Start unrooting  $v$ .
18:   $v.CID \leftarrow \text{reset}$ 
     $v.pointer \leftarrow C$ 
20:
procedure GROWHALF( $v$ )
22:   $v.unrooted \leftarrow \text{false}$ 
    if  $v.active$  and not  $v.whole$  and not  $v.grown$  then
24:  GROW( $v$ )
26:
procedure MERGINGWHOLE( $v$ )
     $v.busy \leftarrow \text{false}$ 
28:  SYNCING( $v$ )
    FLOODINGWHOLE( $v$ )
30:
procedure MERGINGHALF( $v$ )
32:   $v.busy \leftarrow \text{false}$ 
    SYNCING( $v$ )
34:  FLOODINGHALF( $v$ )

```

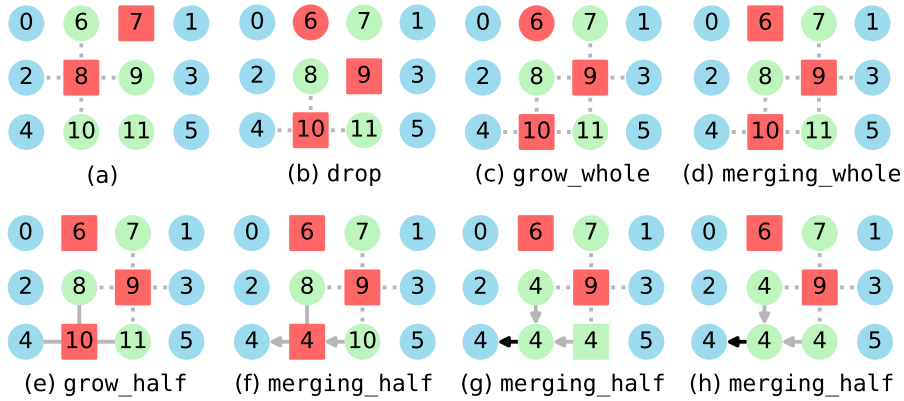


Figure 12: A decoding cycle example for a distance-3 code. Edges are shown as in [Fig. 4](#). Active nodes are squares; inactive nodes, circles. CID is shown as a label. Pointers are shown by arrows on edges. (a) Each node is in its own cluster so has $CID = ID$. Two clusters are active. (b) All relative variables fall by one layer, including CID which is adjusted to refer to the node below. A new defect appears at the top. (c) Node 9 grows its incident edges by $\frac{1}{2}$ as it is active and whole. (d) Node 6 recognises it is a root with a defect, so becomes active. (e) Node 10 grows its incident edges by $\frac{1}{2}$ as it is active and half. Nodes 10 and 11 now each see a lower CID than their own when they look at their neighbours along fully grown edges. (f) They adopt that CID and point toward that neighbour; node 8 thus sees a lower CID than its own. (g) A defect is pushed along a pointer to the root which bitflips an edge. Node 8 updates its CID and pointer, so now the 4-node cluster is fully flooded but not yet fully synced. (h) Throughout this stage, each non-root node was adopting the active variable of the node it was pointing to. This activity propagation now completes, so the 4-node cluster is fully synced.

timesteps. The `merging_whole` stage is the same as `merging_half` but with two extra processes, so we first explain the latter: it comprises two processes, *syncing* and *flooding*, which occur independently. We thus split MERGINGHALF into two subroutines, given in [Algorithm 6](#), effecting each process.

Algorithm 6 Subroutines for [Algorithm 5](#).

```

procedure GROW( $v$ )
2:   for all unfully grown edges  $e$  incident to  $v$  do
   |    $e.growth \leftarrow e.growth + \frac{1}{2}$ 
4:   flip  $v.whole$ 

6: procedure SYNCING( $v$ )
    $x := (v \text{ is a detector}) \text{ and } v.defect$ 
8:   if  $v.pointer = C$  then  $\triangleright v \text{ is a root.}$ 
   |    $v.active \leftarrow x$ 
10:  else
   |    $u := \text{node toward } v.pointer$ 
12:  |    $v.active \leftarrow u.active$ 
   |   if  $x$  then
14:  |   |    $v.busy \leftarrow true$ 
   |   |   flip  $uv.correction$  to push defect to  $u$ 
16:  |   if  $v.active$  changed then
   |   |    $v.busy \leftarrow true$ 
18: procedure FLOODINGWHOLE( $v$ )
20:  if  $v.CID = reset$  then  $\triangleright Finish unrooting v.$ 
   |    $v.busy \leftarrow true$ 
22:  |    $v.CID \leftarrow v.ID$ 
   |    $v.unrooted \leftarrow true$ 
24:  else
   |   for all  $u : uv \in E_W \wedge uv.growth = 1$  do
26:  |   |   if  $u.CID = reset$  then
   |   |   |   if not  $v.unrooted$  then  $\triangleleft$ 
   |   |   |   |    $\triangleright Start unrooting v.$ 
   |   |   |   |    $v.busy \leftarrow true$ 
   |   |   |   |    $v.CID \leftarrow reset$ 
   |   |   |   |    $v.pointer \leftarrow C$ 
   |   |   |   |   break
   |   |   |   else
   |   |   |   |   COMPARE( $u, v$ )
   |   |   |   |   if  $u.grown$  and not  $v.grown$  then
   |   |   |   |   |    $v.busy \leftarrow true$ 
   |   |   |   |   |    $v.grown \leftarrow true$ 
34:  |   |   COMPARE( $u, v$ )
   |   |   if  $u.grown$  and not  $v.grown$  then
   |   |   |    $v.busy \leftarrow true$ 
   |   |   |    $v.grown \leftarrow true$ 
38: procedure FLOODINGHALF( $v$ )
40:  for all  $u : uv \in E_W \wedge uv.growth = 1$  do
   |   COMPARE( $u, v$ )
42: procedure COMPARE( $u, v$ )
44:  if  $u.CID < v.CID$  then
   |    $v.busy \leftarrow true$ 
46:  |    $v.pointer \leftarrow \text{toward } u$ 
   |    $v.CID \leftarrow u.CID$ 

```

D.3 Processes Common to Both Merging Stages

In flooding, newly touching clusters adopt the lowest CID among them. This CID propagates as a flood starting from where they touched: each node looks at its neighbours along fully grown edges. If it sees a lower CID than its own, it adopts that CID and points toward that neighbour ([Lines 44 to 47](#)). After this process, all nodes in a given cluster will have the same CID, and following the pointers will always lead to the root promised by CID.

Remark 3. Crucial to the algorithm is that boundary nodes are of lower ID than detectors. Each root can thus determine if its cluster touches a boundary by checking if itself is a boundary node.

In syncing, all defects are pushed along pointers toward roots, one edge per timestep ([Lines 13 to 15](#)). Eventually, each root will know using [Lemma 1](#) whether its cluster is active ([Line 9](#)). At the same time, this activity knowledge propagates in the opposite direction from root to the rest of the cluster ([Line 12](#)). After this process, a node is in an active cluster iff it is active.

Note that swapping the order of the two subroutines in MERGINGHALF would speed up the stage, as pointers would be updated *before* being used to push defects and backpropagate activity. However, the practicality of this depends on the hardware so in this paper we assume the worse case and perform SYNCING using pointers from the *previous* timestep.

D.4 Processes Unique to `merging_whole`

This subsection will refer to both [Algorithms 5 and 6](#).

D.4.1 Tracking Which Clusters Have Grown

The variable `grown` floods in the same fashion as `cid` but with no connection to pointer ([Algorithm 6 Lines 35 to 37](#)). This ensures all nodes in a given cluster will have the same boolean for `grown`. The memory of whether a cluster has grown resets after each decoding cycle ([Algorithm 5 Line 2](#)).

D.4.2 Unrooting

Unrooting is a process unique to Snowflake and is needed when a downward pointer is dropped to the bottom sheet of W (can happen while a cluster falls out of view). This breaks the pointer tree structure established in the previous decoding cycle, as \exists nonempty $S \subset V_W$ from which following the pointers will lead past the bottom of W . To fix it, each node in S resets its CID and pointer so that the structure can be rebuilt from scratch, via further `merging_whole` timesteps. [Figure 13](#) shows an example.

The breaking point is found immediately after `drop` ([Algorithm 5 Line 17](#)) whence the signal to unroot,

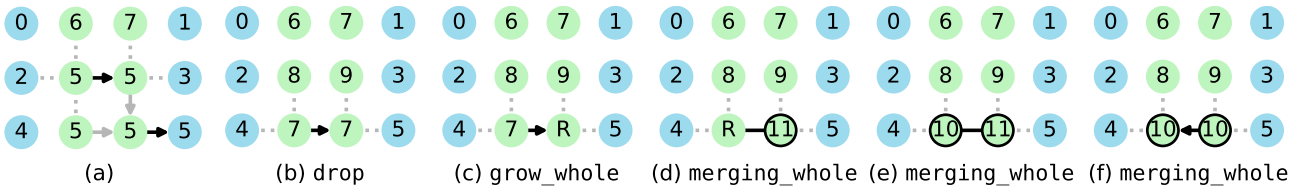


Figure 13: A decoding cycle which demonstrates unrooting. Relative variables are shown as in Fig. 12. CID value reset is labelled 'R'. Nodes with unrooted as true are outlined in black. (a) There is a 5-node cluster. (b) A downward pointer is dropped to the bottom east detector. (c) Thus, this detector starts unrooting. (d) The bottom west detector sees this signal to unroot so starts unrooting. The bottom east detector finishes unrooting. (e) The bottom west detector finishes unrooting. (f) `merging_whole` completes.

`CID = reset`, propagates during `merging_whole` as a flood through the cluster; each node unroots itself as soon as it receives this signal (Algorithm 6 Lines 25 to 32). It takes 2 timesteps for a node to unroot, after which it cannot unroot again in the same decoding cycle (Algorithm 6 Line 27). This ensures the flood does not backpropagate. The memory of whether a node has unrooted resets after this stage finishes (Algorithm 5 Line 22).

The higher up a node is in W , the lower its ID; this is for two reasons. First, it makes unrooting less likely as pointer paths tend to lead upward rather than downward. Second, it ensures defects in active clusters are pushed to a highest point so they can annihilate with defects in newer, smaller clusters as early as possible.